JOURNAL OF GEOPHYSICAL RESEARCH, VOL. 104, NO. B2, PAGES 2797–2816, FEBRUARY 10, 1999

Noise in GPS coordinate time series

Ailin Mao,[1] Christopher G. A. Harrison, and Timothy H. Dixon

Division of Marine Geology and Geophysics, Rosenstiel School of Marine and Atmospheric Sciences
University of Miami, Miami, Florida

Abstract. We assess the noise characteristics in time series of daily position estimates for 23 globally distributed Global Positioning System (GPS) stations with 3 years of data, using spectral analysis and Maximum Likelihood Estimation. A combination of white noise and flicker noise appears to be the best model for the noise characteristics of all three position components. Both white and flicker noise amplitudes are smallest in the north component and largest in the vertical component. The white noise part of the vertical component is higher for tropical stations (±23° latitude) compared to midlatitude stations. Velocity error in a GPS coordinate time series may be underestimated by factors of 5-11 if a pure white noise model is assumed.

1. Introduction

Geophysical studies using geodetic measurements of surface displacement or strain require not only accurate estimates of these parameters but also accurate error estimates. Geodetic measurements of displacement differ in two important ways from other types of geophysical data, and these differences complicate error estimation.

First, we generally require a long time series of measurements, often several years or more, in order to obtain accurate site velocity estimates. This means that a variety of errors with different timescales can corrupt the data. An individual error source may also change with time; for example, the instrument may improve. It is convenient to characterize errors as white (no time dependence) and colored (time-correlated). While the effect of white noise can be greatly reduced through frequent measurement and averaging, this is less useful for time-correlated noise and, in fact, provides no benefit at all for one type of time-correlated noise, the random walk.

Second, while we generally seek to infer the motion of large crustal units, what we actually measure is the motion of a mark or monument on or just below the ground surface. Spurious motion of the mark (monument noise) unrelated to motion of the larger crustal units of interest has been identified as an important noise source for many geodetic measurements [*Johnson and Agnew*, 1995; *Langbein et al.*, 1995]. Analysis of long (decade or more) time series of high-precision two-color electronic distance measurement (EDM) data from sites in California suggests that monument noise can be modeled as a random walk [*Langbein and Johnson*, 1997].

For geodetic data acquired with the Global Positioning System (GPS), a variety of time-correlated processes in addition to monument noise corrupt velocity estimates and, in fact, likely dominate the error budget at the present time. In other words, GPS velocity estimates may not yet be accurate enough to observe monument noise except in extreme cases. Other sources of time-correlated noise include mismodeled satellite orbits, other reference frame effects (e.g., Earth orientation), mismodeled atmospheric effects, and mismodeled antenna phase center effects, which may vary with satellite elevation, azimuth, and local environmental factors.

Studies of time-correlated noise in GPS time series have been hampered by the relatively short time that high-quality time series have been available. Rigorous analysis of time-correlated noise in GPS data may well require decade or longer time series, but high-precision results from continuously operating stations have been available only since about 1992 or 1993. The present study reports the noise characteristics of 23 globally distributed GPS sites that have operated more or less continuously for about 3 years.

2. Previous Work

Zhang et al. [1997] analyzed 1.6 years of essentially continuous daily measurements from 10 sites in southern California, and the reader is referred to that work for additional background on some of the issues discussed here. *Zhang et al.* [1997] were able to reduce regionally correlated noise (probably dominated by orbit errors) by use of a filtering algorithm that subtracted common mode, nontectonic signals from the GPS time series [*Wdowinski et al.*, 1997]. This method is applicable whenever data from a relatively dense network are available but is not yet possible for a globally distributed set of sites, because of their isolation. Noise in the residual time series studied by *Zhang et al.* [1997] was characterized as "fractal white" (spectral index 0.4, defined below) or a combination of white noise and flicker noise (spectral indices of 0 and 1, respectively). Given the shortness of the time series available to them, *Zhang et al.* [1997] could not distinguish between these models.

This study differs in three ways from that of *Zhang et al.* [1997]. First, we study a global distribution of sites (Figure 1), which allows us to assess regional differences in noise. This is important for the GPS, where orbit, reference frame, and atmospheric errors are likely to be important and may exhibit regional differences. Second, we have studied "raw" GPS coordinate time series, as opposed to data with orbit and reference frame errors reduced or eliminated through common mode techniques. Thus our results should be applicable to GPS coordinate time series from any site, no matter how isolated. Filtered data or relative position (baseline) data can be expected to be less noisy than results presented here, provided the baselines are short enough.

[1]Now at Magellan Systems Corporation, San Dimas, California.

Copyright 1999 by the American Geophysical Union.

Paper number 1998JB900033.
0148-0227/99/1998JB900033$09.00

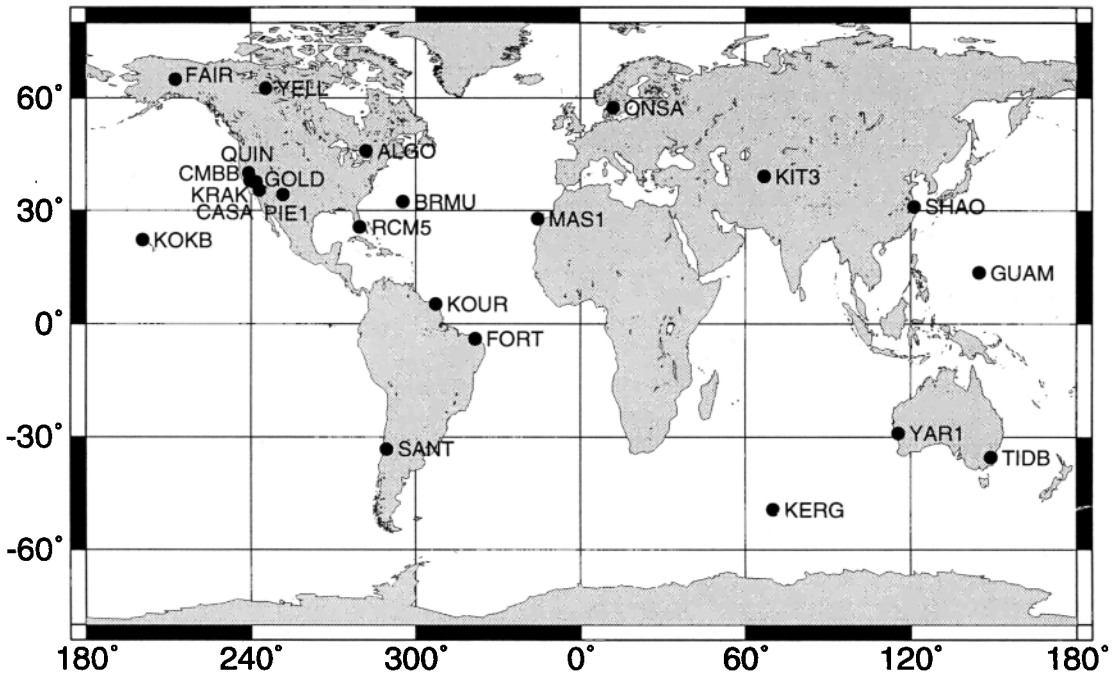

Figure 1. Distribution of Global Positioning System stations used in this study.

Third, longer time series (3.0 years, nearly a factor of 2 longer) are now available, enabling a more accurate assessment of long-period time-correlated noise.

3. Data Analysis

Since early 1994, GPS data from a number of continuously operating stations (currently 120) have been analyzed in the Geodesy Laboratory of the University of Miami to study various geophysical phenomena. We selected 23 stations with time spans longer than 2.5 years for noise analysis (Table 1, Figure 1). Seventeen stations have 3.0 years of data or more. The 1994 and later period used here is a convenient one. Many stations experienced frequent equipment changes prior to 1994. Also, these later data tend to be less noisy compared to earlier data, especially in the Southern Hemisphere, perhaps reflecting improvement in satellite ephemerides as the number of global tracking stations increased rapidly between 1991 and 1994.

To speed analysis, for most applications (and this analysis) we use satellite orbit and clock files provided by the Jet Propulsion Laboratory (JPL) [*Zumberge et al.*, 1997]. The resulting daily station coordinates are transformed into global reference frame ITRF-94 [*Boucher et al.*, 1996]. Analysis procedures are described by *Dixon et al.* [1997].

We use two methods, spectral analysis and Maximum Likelihood Estimation (MLE), to assess time-correlated noise in these time series. We use spectral analysis to estimate the spectral index of noise, while MLE is used to characterize the amplitudes of the stochastic processes with integer spectral indices.

3.1. Spectral Analysis

The power spectra, P, of many geophysical phenomena are well approximated by a power-law dependence on frequency f of the form [*Agnew*, 1992]

$$P(f) = P_0 f^{-\alpha} \tag{1}$$

where α is the spectral index and P_0 is a constant. Larger α implies a more correlated process and more relative power at lower frequencies. White noise has a spectral index of 0, flicker noise has a spectral index of 1, and a random walk has a spectral index of 2.

Spectral indices need not be limited to integer values. Geophysical phenomena and noise with fractional spectral indices in the range $1<\alpha<3$ are termed "fractal random walk," while indices in the range $-1<\alpha<1$ are termed "fractal white noise" [*Agnew*, 1992]. Noise processes with $-1<\alpha<1$ are stationary, while processes with spectral index larger than 1 are nonstationary. A stationary random process is one whose statistical properties (e.g., mean and variance) are invariant in time.

Following *Langbein and Johnson* [1997], the spectrum of a set of measurements can be modeled as the sum of white noise and colored noise:

$$P(f) = P_0\left(f^{-\alpha} + f_0^{-\alpha}\right) \tag{2}$$

where f_0 is the crossover frequency of the power spectrum defined as the point at which the two processes have the same power levels. The constants α, P_0, and f_0 can be estimated by fitting a curve to the power spectrum of a time series. The uncertainties are determined by seeing how well the model fits the spectrum using standard least squares. We have used an iterative nonlinear least squares method to estimate these parameters. In order to speed convergence, we apply the natural logarithm to both sides of (2):

$$\ln P(f) = \ln P_0 + \ln(f^{-\alpha} + f_0^{-\alpha}) \tag{3}$$

The differential form of this equation can be written

$$d\{\ln[P(f)]\} = d\ln(P_0) - \frac{\alpha f_0^{-\alpha-1}}{f^{-\alpha} + f_0^{-\alpha}} df_0 + \frac{f^{-\alpha}\ln f + f_0^{-\alpha}\ln f_0}{f^{-\alpha} - f_0^{-\alpha}} d\alpha \tag{4}$$

Using the relationship between parameters and measurements given in (4), we can form a set of observation equations, $\mathbf{AX} = \mathbf{V}$,

Table 1. Station Description (Post-1994)

ID	Station Name	Lat, deg	Long, deg	H,[a] m	Receiver[b]	Antenna[c]
ALGO	Algonquin	45.96	-78.07	202	TR	TR
BRMU	Bermuda	32.37	-64.70	-8	TR	TR
CASA	Mammoth Lakes	37.64	-118.10	2390	TR	TR; add antenna skirt (1)
CMBB	Columbia	38.03	-120.39	695	Ashtech Z-12	Ashtech; TR (2)
FAIR	Gilmore Creek	64.98	-147.50	319	ROGUE; TR(3)	ROGUE; TR(3)
FORT	Fortaleza	-3.88	-38.42	20	TR	TR
GOLD	Goldstone	35.42	-116.89	987	ROGUE	ROGUE; TR (4)
GUAM	Guam	13.59	144.87	202	TR	TR
KERG	Kerguelen Island	-49.35	70.26	74	ROGUE	TR
KIT3	Kitab	39.14	66.88	643	TR	TR
KOKB	Kokee Park	22.13	-159.66	1167	ROGUE; TR(5)	ROGUE; TR(5)
KOUR	Kourou	5.25	-52.81	-25	ROGUE	ROGUE
KRAK	Krakatua	37.71	-118.88	2359	TR	TR
MAS1	Maspalomas	27.76	-15.63	197	TR	TR
ONSA	Onsala	57.40	11.92	46	TR	ROGUE
PIE1	Pietown	34.30	-108.12	2347	TR	TR
QUIN	Quincy	39.97	-120.94	1106	TR	TR
RCM5	Richmond	25.61	-80.38	-25	TR	TR
SANT	Santiago	-33.15	-70.67	723	ROGUE; TR(6)	ROGUE; TR(6)
SHAO	Shanghai	31.10	121.20	22	TR	TR
TIDB	Tidbinbilla	-35.40	148.98	665	ROGUE	ROGUE; TR(7)
YAR1	Yaragadee	-29.05	115.35	241	ROGUE	ROGUE
YELL	Yellowknife	62.48	-114.48	181	TR	TR

[a]Height above ellipsoid.
[b]Receiver: ROGUE, ROGUE SNR-8; TR, ROGUE SNR-8000 or SNR-8100. Numbers in parentheses are equipment change dates: (1) June 3, 1995; (2) Aug. 20, 1997; (3) April 16, 1996; (4) Oct. 31, 1995; (5) Jan. 10, 1996; (6) July 17, 1996; (7) June 26, 1996.
[c]Antenna: ROGUE, DORNE MARGOLIN R; TR, DORNE MARGOLIN T; Ashtech, Ashtech GEODETIC L1/L2 P. Numbers in parentheses are equipment change dates (see previous note).

where A is a function of P_0, f_0 and α, $\mathbf{X}=[d\ln(P_0), df_0, d\alpha]^T$ is the update vector for parameters, and $\mathbf{V}$ is the difference between the observed and the computed power spectra. A normal equation can be created based on least-squares in the form

$$\mathbf{NX} = \mathbf{L} \tag{5}$$

where the normal matrix $\mathbf{N} = \mathbf{A}^T\mathbf{A} = [n_{ij}]$ and vector $\mathbf{L} = \mathbf{A}^T\mathbf{V} = [l_i]$. The Levenberg-Marquardt method [*Press et al.*, 1992] is used to solve the nonlinear parameter estimation. The normal matrix here gives only the trend at a particular point, but not how far that slope extends. We can replace the normal matrix $\mathbf{N}$ in (5) with a new matrix $\mathbf{N}' = [n'_{ij}]$ defined by the following rules:

$$n'_{ij} = \begin{cases} n_{ij}(1+\lambda) & i = j \\ n_{ij} & i \neq j \end{cases} \tag{6}$$

When λ is very large, the matrix $\mathbf{N}'$ is forced to be nearly diagonal, and the step size by which the solution is approached is reduced because the diagonal elements of the normal matrix are enlarged. On the other hand, as λ approaches zero, $\mathbf{N}'$ will be close to the real normal matrix $\mathbf{N}$.

Given an initial guess for the set of fitted parameters $\mathbf{X}$, we use the following iterative steps modified from the Levenberg-Marquardt method:

1. Pick a modest value for λ, say $\lambda = 0.001$.
2. Compute normal matrix $\mathbf{N}$, $\mathbf{L}$ and misfit $\chi^2(X)$.
3. Modify the normal matrix as in (6) and solve the modified normal equation (5) for δX and evaluate $\chi^2(X+\delta X)$.
4. If $\chi^2(X+\delta X) \geq \chi^2 X$, increase λ by a factor of 10 and go back to step 3.
5. If $\chi^2(X+\delta X) < \chi^2 X$, update the trial solution with $X+\delta X$, decrease λ by a factor of 10, and go back to step 2.
6. The iteration can be stopped when $\chi^2(X+\delta X)$ decreases by a negligible amount for $\lambda \leq 0.01$.

For example, when α=1, (2) approaches P_0/f at low frequencies, which corresponds to flicker noise, and approaches a constant P_0/f_0 at high frequencies, which corresponds to white noise. The amplitudes of white noise and flicker noise components can be calculated from estimated values of P_0 and f_0, and similarly

for the case of random walk noise (α=2) or arbitrary α. Noise components derived in this way are less precise than those derived with the MLE techniques described later, although they can provide an independent estimate for comparison purposes.

In our case, α and P_0 vary by less than 10, while f_0 is much more variable and may cause convergence problems, especially if it is close to zero (white noise dominates over time-correlated noise). In case of divergence, a straight line can be fitted to the spectrum to estimate the spectral index, although this may underestimate the spectral index at low frequency for time series composed of white noise plus time-correlated noise. Again, reference to MLE allows an independent estimate.

Time series are windowed prior to spectral analysis. The simplest window is a boxcar window, in which the finite data set is left alone. Specialized windows can be used to reduce spectral leakage and sidelobe effects [*Press et al.*, 1992], but can sometimes artificially enhance the power at low frequencies, which is undesirable for our application. Boxcar windows were used for most of the results presented here. To verify the stability of our spectral estimates, we also analyzed the time series using several other common windowing techniques. In general, these gave similar results to the boxcar window results, as described below (section 4.1.).

Two techniques (Fourier spectrum and least squares) can be used to estimate the periodogram of a time series, depending on whether the data are evenly spaced or not. For a series of N discrete observations x_j (j = 1, N) at equal spacing, the power spectrum by means of a periodogram is defined from the discrete Fourier transform as [*Scargle*, 1982]

$$P(f_n)=\frac{1}{N}\left[\left(\sum_{j=1}^{N} x_j \cos 2\pi j f_n\right)^2+\left(\sum_{j=1}^{N} x_j \sin 2\pi j f_n\right)^2\right] \quad (7)$$

where $f_n = n/T$, T is the fundamental period, and n = 1, ..., N/2. If x_j is pure white noise, $P(f_n)$ is an exponentially distributed random variable with an expectation value equal to the variance of the white noise. The amplitude estimates of the spectrum at the frequencies f_n are independent.

In many situations (including many of our GPS time series), evenly spaced data cannot be obtained. There are ways to modify unevenly spaced time series to simulate evenly spaced ones. Interpolation is one approach, but most interpolation techniques perform poorly for large gaps [*Press et al.*, 1992], a problem at some of the GPS sites. We follow the approach of *Lomb* [1976], who used a nonlinear least squares technique to estimate spectra by fitting sine waves directly to the data. Given a set of N observations x_j with zero mean at t_j (j = 1 to N), we can set up the following model at a given frequency f:

$$x_j+\varepsilon_j = a\cos 2\pi(t_j-\tau)f + b\sin 2\pi(t_j-\tau)f \quad (8)$$

where the errors ε_j are independent and have zero mean and common variance, a and b are unknowns, and τ is introduced for simplification, defined by

$$\tan(4\pi f\tau) = \sum_{j=1}^{N} \sin 4\pi t_j f \Big/ \sum_{j=1}^{N} \cos 4\pi t_j f \quad (9)$$

Then the periodogram can be derived as follows:

$$P(f)=\frac{1}{2}\left\{\frac{\left[\sum_{j=1}^{N} x_j \cos 2\pi(t_j-r)f\right]^2}{\sum_{j=1}^{N}\cos^2 2\pi(t_j-\tau)f}+\frac{\left[\sum_{j=1}^{N} x_j \cos 2\pi(t_j-r)f\right]^2}{\sum_{j=1}^{N}\sin^2 2\pi(t_j-\tau)f}\right\} \quad (10)$$

Scargle [1982] proved that the resulting periodogram has exactly the same exponential probability distribution as for evenly spaced data. Windowing techniques can also be applied. While this expression can be evaluated at any frequency, it is typically evaluated only at a set of evenly spaced frequencies similar to the Fourier spectrum, defined by

$$f_n = n/T \qquad n = 1, 2, \ldots \quad (11)$$

where T is the fundamental period. However, the orthogonality of the periodogram at these frequencies is lost for unevenly spaced data. It can be shown by numerical test or derivation that the Fourier spectrum and least squares method are equivalent when both are applied on the same evenly spaced data [*Scargle*, 1982].

To verify the performance of the least squares algorithm in the presence of data gaps, we tested it with two kinds of missing data: small amounts of missing data randomly distributed through the time series, and a single large gap. For the first test we randomly removed 30% of the data from an evenly spaced time series and found that there is essentially no bias in the resulting spectral profile, compared with the spectrum estimated from the original time series (Figure 2).

To test the effect of large gaps in the data, we generated 20 synthetic time series of 1000 points each, with noise characteristics similar to our GPS time series (spectral indices 0.80-1.60), removing 10, 20, and 30% of the data from each time series near the beginning (100 points in) to simulate a large gap. Effects on the estimated spectral indices for individual time series were always less than 0.4: +0.24 to -0.20 for 10% data removal; and +0.27 to -0.39 for 20% data removal; +0.37 to -0.34 for 30% data removal. Effects on the mean spectral index were negligible: +0.002 for 10% data removal; -0.06 for 20% data removal; and +0.01 for 30% data removal. We conclude that our technique for estimation of the spectral indices of time series is robust in the presence of data gaps.

For relatively short time series the spectral index can be underestimated. We have investigated our sensitivity to this effect in two ways. First, the nonlinear least squares estimation method was tested on theoretical power-law spectra with different lowest frequency. Spectral indices of 2 and 1 were tested. Nonlinear least squares can estimate the spectral index reliably when the length of the time series is 1.8 times the crossover period for both index values.

We further tested both the Fourier method and least squares method on mixed noise synthetic time series, mixing white noise

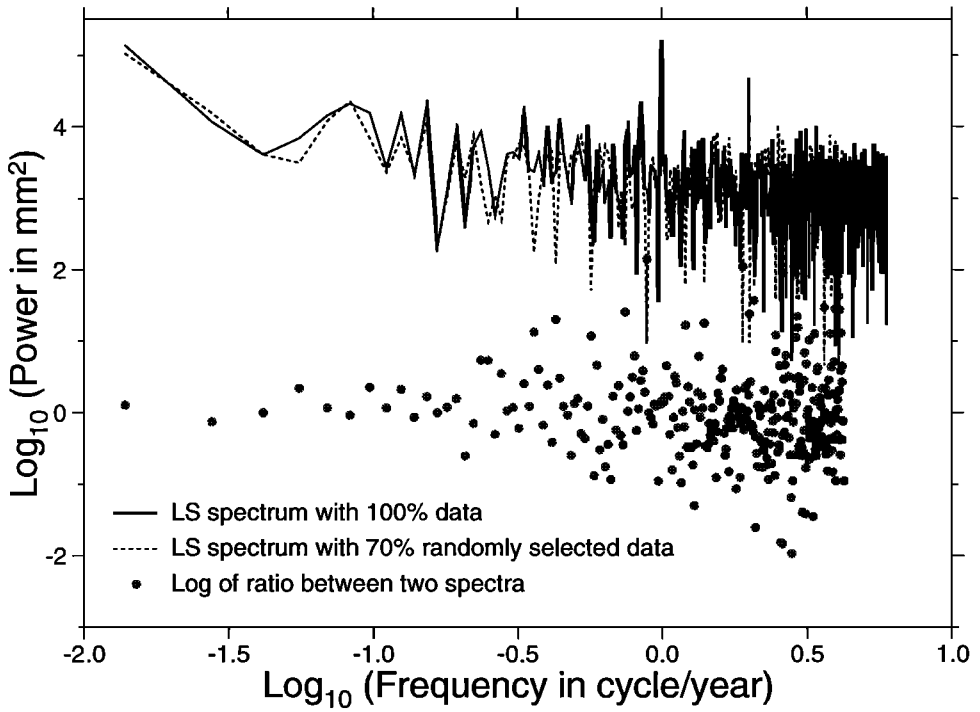

Figure 2. Power spectrum computed from complete time series (solid line) compared with spectrum computed with 30% of data randomly removed. Data are 73 years of monthly mean tide gauge data from Boston. An annual and semiannual term stand out above the noise. Frequency is in cycles per year.

with either flicker noise or random walk noise, with similar amplitudes to current GPS time series (Table 2). In test case one, time series were simulated with 4.0 mm of white noise and 5.0 mm of flicker noise, and 30% of the points randomly removed. The crossover period of these time series is about 20 days. We found that the spectral indices can be estimated reliably for time series longer than 2 years, a criterion we meet for all our time series. Although the mean estimation is not biased for time series equal to 1 year, many solutions failed to converge. We also found that it is more difficult to estimate the spectral index when we removed the annual term. In test case two we simulated GPS time series with 4.5 mm of white noise and 1.5 mm/$\sqrt{\text{yr}}$ of random walk noise, whose crossover period is about 1 year. The length of data required to characterize accurately the random walk component is usually taken to be 5 times the crossover period ($5/f_0$), in this case 5 years. However, in this simulation, even 5 years was inadequate. Periodic signals and other noise make it more difficult to detect random walk noise, implying that it will be some time before GPS time series can be analyzed for accurate estimates of random walk noise, at least for data similar to the coordinate time series discussed here. For more precise baseline (relative position) data, random walk noise may be characterized in less time, depending on its amplitude (e.g., Dixon et al., 1997). Spectral index results are summarized in Table 3.

3.2. Maximum Likelihood Estimation

Assuming the observed time series $\mathbf{X}=\{ x_j, t_j\ (j=1, N) \}$ is composed of only white noise with variance σ_w^2, flicker noise with variance σ_f^2 (its scale will be defined later), and random-walk noise σ_{rw}^2 (variance over specific time, e.g., 1 year), the covariance matrix of observations can be written as

$$\mathbf{Q}_{xx} = \sigma_w^2\mathbf{I} + \sigma_{rw}^2\mathbf{R}_{rw} + \sigma_f^2\mathbf{R}_f \tag{12}$$

where $\mathbf{I}$ is the $N \times N$ identity matrix, and $\mathbf{R}_{rw}$ and $\mathbf{R}_f$ are the matrices representing the covariance of random walk noise and flicker noise, respectively.

A random walk process is derived by integrating white noise. As we do not have any information about the random walk process before the observations start, we assume that random walk noise at time t_0 is equal to zero. With this assumption the observed time series over a fixed time T is stationary (even though the process itself is not) and easily characterized statistically [*Brockwell and Davis*, 1996]. The matrix $\boldsymbol{R}_{rw}$ can be expressed as the following equation [*Johnson and Wyatt*, 1994]:

$$\mathbf{R}_{rw} = \begin{pmatrix} \Delta t_1 & \Delta t_1 & \cdots & \Delta t_1 \\ \Delta t_1 & \Delta t_2 & \cdots & \Delta t_2 \\ \vdots & \vdots & \ddots & \vdots \\ \Delta t_1 & \Delta t_2 & \cdots & \Delta t_n \end{pmatrix} \tag{13}$$

where $\Delta t_j = t_j - t_0$.

For flicker noise ($\alpha = 1$) the elements of matrix $\boldsymbol{R}_f$ can be approximated by [*Zhang et al.*, 1997]

$$r_{ij} = \begin{cases} \left(\frac{3}{4}\right)^2 \times 2 & t_i = t_j \\ \left(\frac{3}{4}\right)^2 \times \left(2 - \frac{\log\left|t_i - t_j\right| / \log 2 + 2}{12}\right) & t_i \neq t_j \end{cases} \tag{14}$$

for most space geodetic time series ($|t_i - t_j| << 2^{22}$). The first several elements look like

Table 2. Test Results of Spectral Analysis on Synthetic Time Series

	Length of Time Series					
	1 year	2 years	3 years	5 years	8 years	15 years
			Test Case One: White Plus Flicker Noise			
Mean ± standard deviation	1.22±0.50	1.12±0.40	1.15±0.32	1.08±0.25	1.07±0.15	1.10±0.11
Converged solutions	29	40	40	40	40	40
			Test Case One With Annual Term Removed			
Mean ± standard deviation	0.77±0.27	0.67±0.25	0.82±0.31	0.83±0.17	0.92±0.17	1 02±0.00
Converged solutions	15	31	36	40	40	40
			Test Case Two: White Noise Plus Random Walk Noise			
Mean ± standard deviation	0.91±0.63	1.42±1.23	1.81±1.41	1.48±0.63	1.68±0.62	1.99±0.42
Converged solutions	9	16	30	34	40	40
			Test Case Two With Annual Term Removed			
Mean ± standard deviation	-	0.13±0.11	1.55±2.09	1.52±1.22	2.20±1.02	2.30±0 52
Converged solutions	0	3	6	13	29	39

A total of 40 simulations are tested for each solution. In test case one, time series are simulated with 4.0 mm of white noise and 5.0 mm of flicker noise; 30% of the points are randomly taken away The crossover period of such a time series is about 19 days. In test case two we simulate GPS time series with 4.5 mm of white noise and 1.5mm/√yr of random walk noise, whose crossover period is about 1 year.

$$\mathbf{R_f} = \begin{pmatrix} 1.125 & 1.031 & 0.984 & \cdots \\ 1.031 & 1.125 & 1.031 & \cdots \\ 0.984 & 1.031 & 1.125 & \cdots \\ \vdots & \vdots & \vdots & \ddots \end{pmatrix} \quad (15)$$

The constants in (14) are chosen such that flicker noise and random walk noise, with equal variance and a sampling interval of 1 day, have equivalent power levels over a period of 1 year. The scale of flicker noise is also defined by (14).

The σ_w, σ_{rw}, and σ_f can be estimated by finding those values that maximize the following likelihood function, which is the joint probability of the data set [*Langbein and Johnson*, 1997]:

$$L(\mathbf{X},\sigma_w,\sigma_{rw},\sigma_f) = (2\pi)^{-N/2}\left|\mathbf{Q}_{XX}\right|^{-1/2}\exp\left(-\frac{1}{2}\mathbf{X}\mathbf{Q}_{XX}^{-1}\mathbf{X}\right) \quad (16)$$

Applying natural logarithms to both sides, we obtain

$$\ln L(\mathbf{X},\sigma_w,\sigma_{rw},\sigma_f) = -\frac{N}{2}\ln(2\pi) - \frac{1}{2}\ln\left|\mathbf{Q}_{XX}\right| - \frac{1}{2}\mathbf{X}\mathbf{Q}_{XX}^{-1}\mathbf{X} \quad (17)$$

For most available time series, only one of σ_{rw} and σ_f can be estimated along with σ_w. We can use the preceding spectral analysis as a guide to an appropriate noise model. Alternately, we can use MLE to test several noise models (e.g., white plus flicker, white plus random walk), and choose the optimum model on the basis of the maximum likelihood value [*Langbein and Johnson*, 1997; *Zhang et al.*, 1997]. We used both approches. The maximum likelihood problem can be solved in several ways [e.g., *Koch*, 1986; *Press et al.*, 1992]. We selected the downhill simplex method developed by Nelder and Mead [*Press et al.*, 1992]. The method requires only function evaluations, not derivatives, although it is not very efficient in terms of the number of function evaluations required. The algorithm starts with an initial guess of an N vector of independent parameters, then moves down through the complexity of an N-dimensional topography until reaching a minimum. Each step, called a reflection, moves the point of the simplex, where the function is largest or highest, through the opposite face of the simplex to a lower point.

Langbein and Johnson [1997] tested the MLE technique described here with synthetic time series with known amounts of white and random walk noise and showed that MLE recovers reasonable estimates of the magnitude of white and random walk noise and uncertainties. With slight modification their algorithm can also recover flicker noise magnitude and uncertainty. Table 4 shows the results of simulations for 10 time series, each with 5 mm of white noise and 5 mm of flicker noise. It is clear that the algorithm is able to recover reasonable estimates of white and flicker noise as well as reasonable uncertainty estimates.

4. Results and Discussion

4.1. Spectral Index and Noise Amplitude

The GPS position time series for all three components of the 23 stations are illustrated in Figure 3. Time series were detrended before spectral analysis and Maximum Likelihood Estimation. Data points with residuals larger than 3 times the standard error are treated as outliers and removed in the linear regression. Figure 4 shows the power spectra of the same time series. Most of the spectra can be described as white (constant power) at short periods (high frequency), and red (more power) at longer periods (low frequency) (e.g., ALGO east). Most of the spectra are white for periods shorter than about 15-30 days (Figure 4). However, a few of the spectra can equally well be described as "fractal white" with power rising uniformly on these log-log plots toward higher values at longer periods (e.g., CMBB east). The best fitting white plus colored noise spectrum is shown on each plot if convergence was achieved. The value of

Table 3. Station Time Series: Length and Spectral Index Estimates

ID	Span, years	Points	North, [1] α	East, [1] α	Vertical, [1] α
ALGO	3.4	864	1.38±0.56	1.63±0.70	0.69±0.21
BRMU	3.6	803	-	1.66±0.50	2.17±0.80
CASA	3.4	801	1.22±0.56	0.70±0.19	0.87±0.48
CMBB	3.3	498	0.71±0.55	-	1.17±0.43
FAIR	3.4	381	0.54±0.38	-	1.10±0.81
FORT	3.8	589	0.93±0.45	0.95±0.62	0.61±0.55
GOLD	3.6	487	-	1.06±0.45	1.06±0.54
GUAM	2.8	681	-	-	-
KERG	2.6	762	0.91±0.18	1.04±0.57	1.91±1.50
KIT3	2.7	620	0.86±0.20	0.79±0.47	1.03±0.46
KOKB	3.4	824	1.30±0.56	0.53±0.22	1.39±0.41
KOUR	3.6	627	-	0.75±0.42	0.74±0.32
KRAK	2.9	627	1.13±0.23	0.51±0.34	0.83±0.28
MAS1	3.0	581	1.47±0.62	0.55±0.31	1.04±0.25
ONSA	3.2	524	1.14±0.40	0.91±0.32	1.13±0.45
PIE1	3.6	606	-	0.75±0.40	1.24±0.59
QUIN	3.4	818	1.47±0.66	1.23±0.44	0.83±0.42
RCM5	2.7	554	-	0.52±0.59	1.34±0.64
SANT	3.6	568	0.56±0.48	0.61±0.42	1.56±0.73
SHAO	2.8	764	0.81±0.44	-	1.49±0.63
TIDB	3.4	853	1.41±0.50	0.74±0.43	1.15±0.47
YAR1	3.4	833	-	0.64±0.35	0.63±0.67
YELL	3.4	538	-	0.68±0.28	0.93±0 64
Weighted mean[2]			0.97±0.24	0.74±0.26	0.97±0.29

[1]No entry indicates failure to converge.
[2] Uncertainty is weighted rms scatter about weighted mean.

Table 4. Results of Tests of MLE Algorithm on Synthetic Time Series Containing 5 mm of White Noise and 5 mm of Flicker Noise

Run	White Noise, mm	Flicker Noise, mm
1	5.03±.22	5.69±.69
2	5.10±.20	4.47±.52
3	4.97±.21	5.27±.76
4	5.32±.22	4.37±.85
5	5.05±.20	3.68±.47
6	4.99±.20	4.32±.76
7	5.05±.22	5.72±.79
8	5.21±.21	3.98±.66
9	5.26±.22	4.97±.64
10	4.85±.22	6.17±.63

Uncertainties are 1 standard error. MLE, Maximum Likelihood Estimation.

the spectral index, α, and its standard error are also shown. Table 3 shows the spectral index estimates for the north, east, and vertical components. The spectral indices range from 0.51 to 2.17. By individual components, the weighted means are 0.97±0.24 (north), 0.74±0.26 (east), and 0.97±0.29 (vertical). Thus there is no significant difference in the spectral character of noise for north, east and vertical components. The weighted mean for all three components is 0.89±0.28, and the unweighted mean of all components is 1.02±0.37. The most reliable estimates for spectral index (uncertainty less than or equal to 0.50) lie in the range of 0.51 - 1.66. Since the mean spectral index is close to 1.0 regardless of component or weighting, we suggest that flicker noise is an adequate model for time-correlated noise in these time series. However, we cannot preclude the possibility that $\alpha < 1.0$ or $\alpha > 1.0$ (fractal white noise or fractal random walk noise), given the uncertainties.

To check the reliability of our spectral index estimates, we calculated the indices in several different ways. The mean values quoted above are based on nonwindowed data, with no value

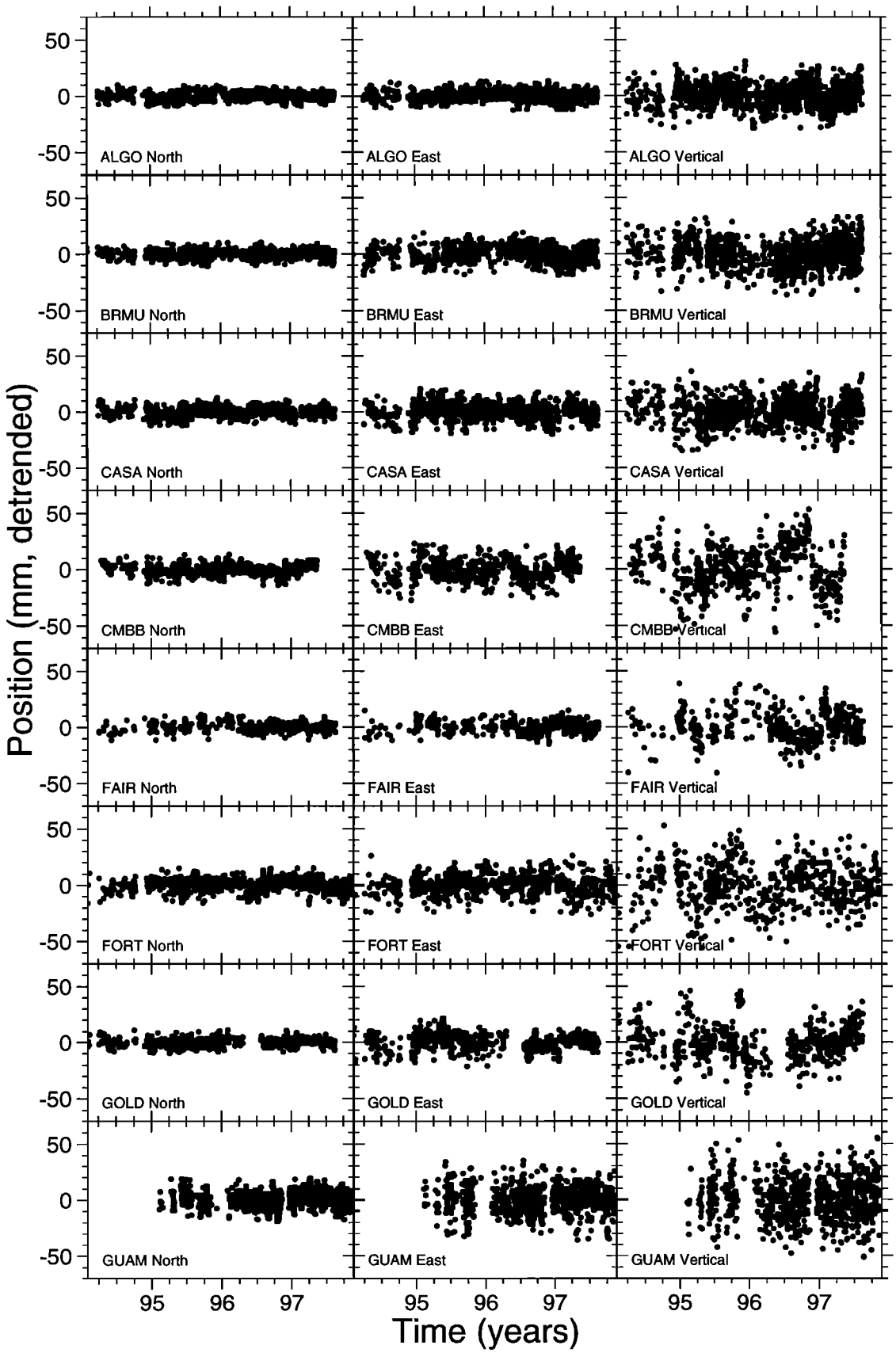

Figure 3. PS coordinate time series used in this study. Horizontal axes are for the years of about 1994-1998. Vertical axes are north, east, and vertical components in mm, offset by a nominal value.

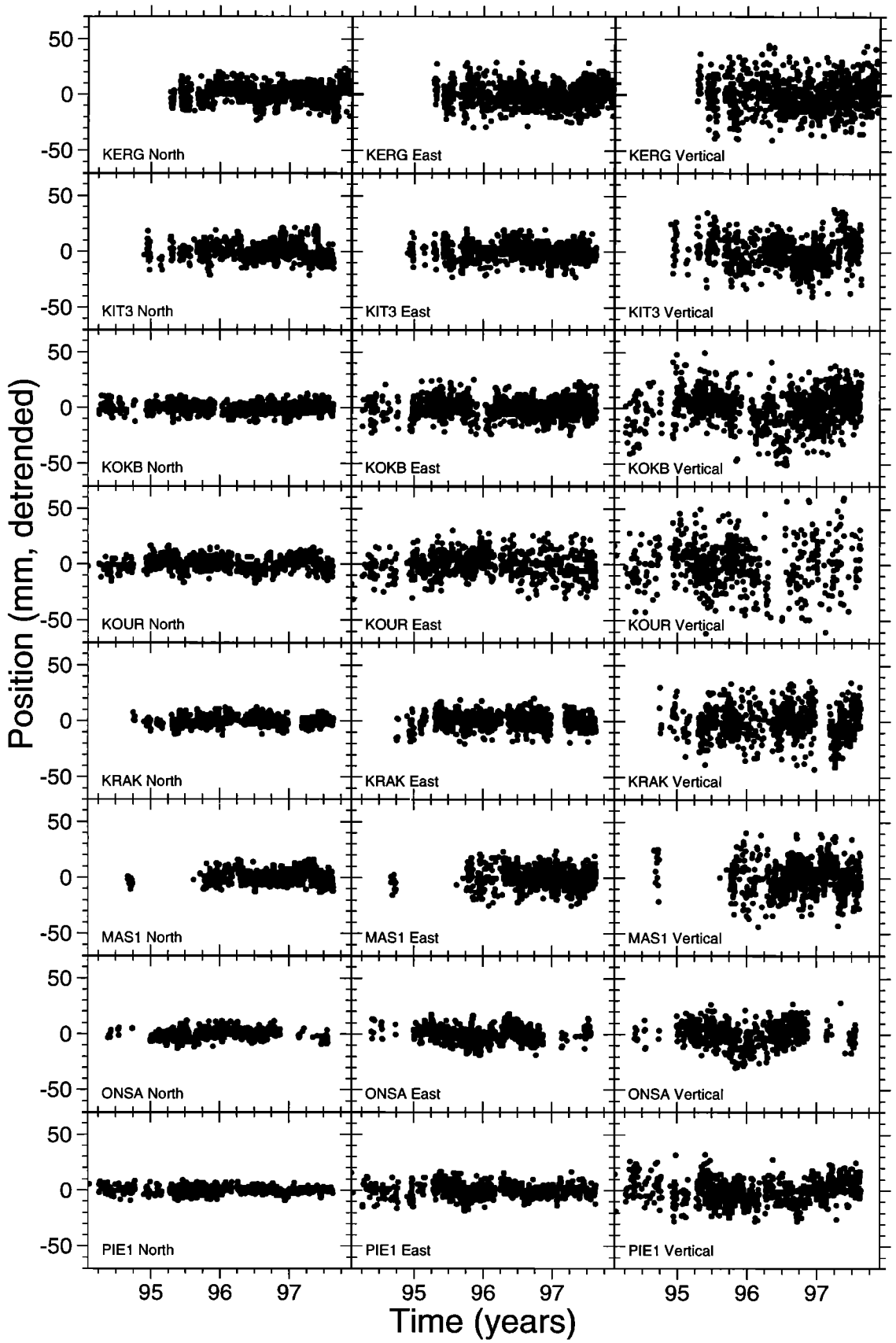

Figure 3. (continued)

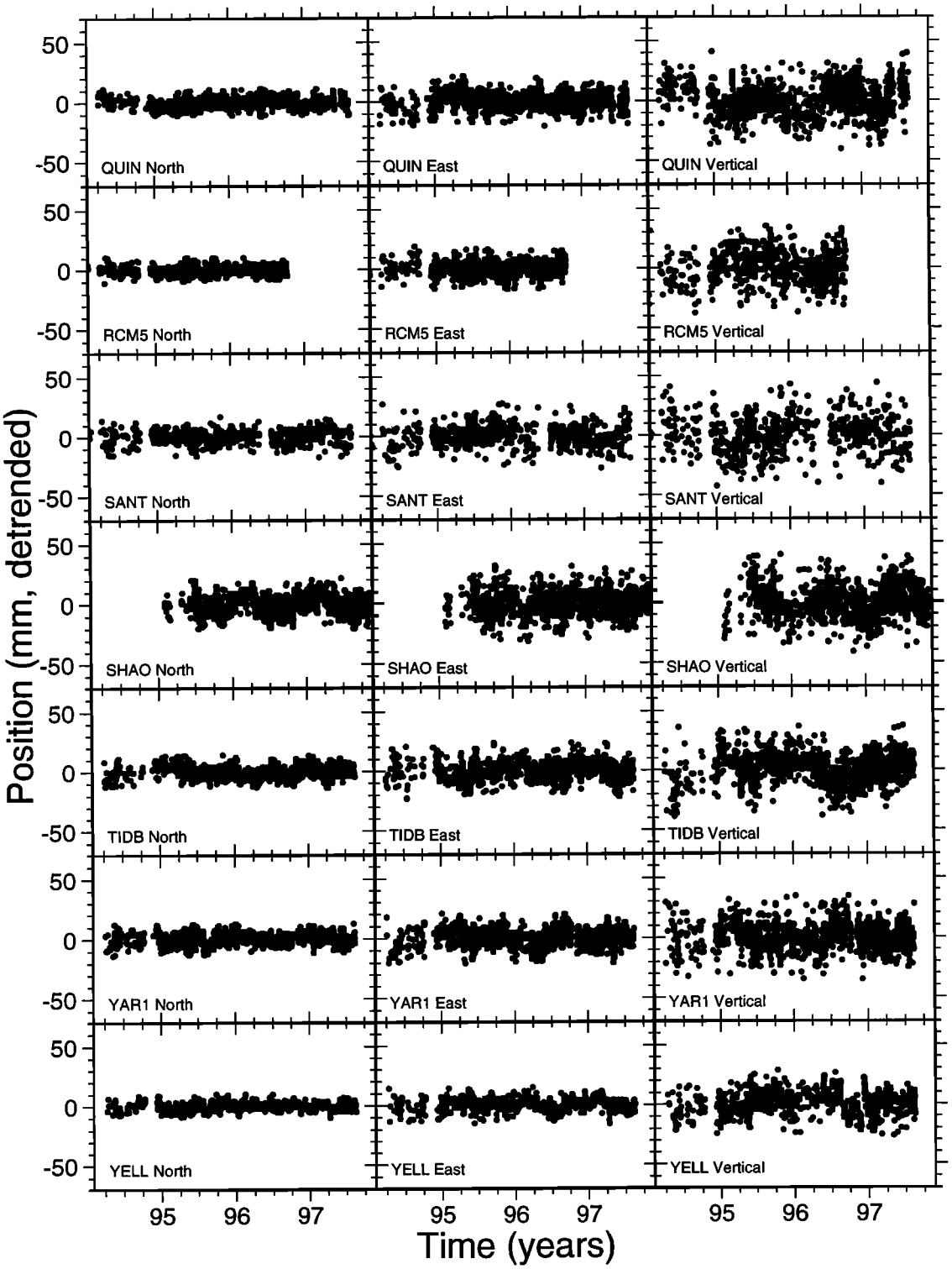

Figure 3. (continued)

computed for time series that failed to converge (13 out of 69 estimates; Table 3). It is possible to approximate the spectra for these divergent series by fitting a straight line. Employing this approach, again with non-windowed data, yields a mean spectral index of 0.98±0.42. We also computed spectra using several windowing techniques [*Press et al.*, 1992]. Use of the Hanning window gives a mean spectral index of 0.95±0.46, while use of the Welch window gives 0.90±0.41.

We tested solutions with and without an annual term removed. For most solutions the results are equivalent within errors. However, when the annual term is removed, a larger number of solutions failed to converge. For the spectral index results discussed

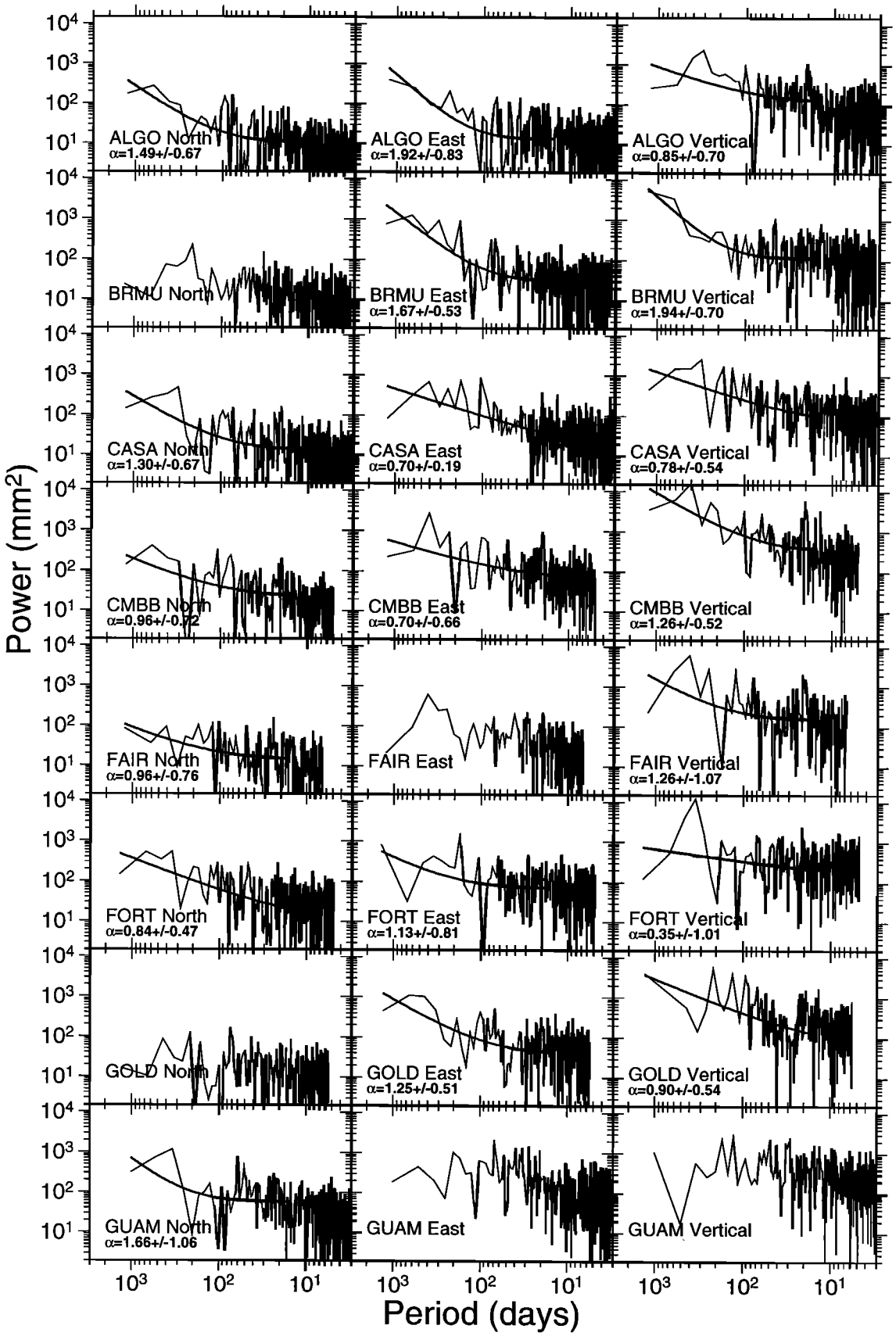

Figure 4. Power spectra of GPS time series shown in Figure 3. Here α is estimated spectral index. Horizontal axes are period in days. Vertical axes are power in mm^2. Missing values indicate failure to converge.

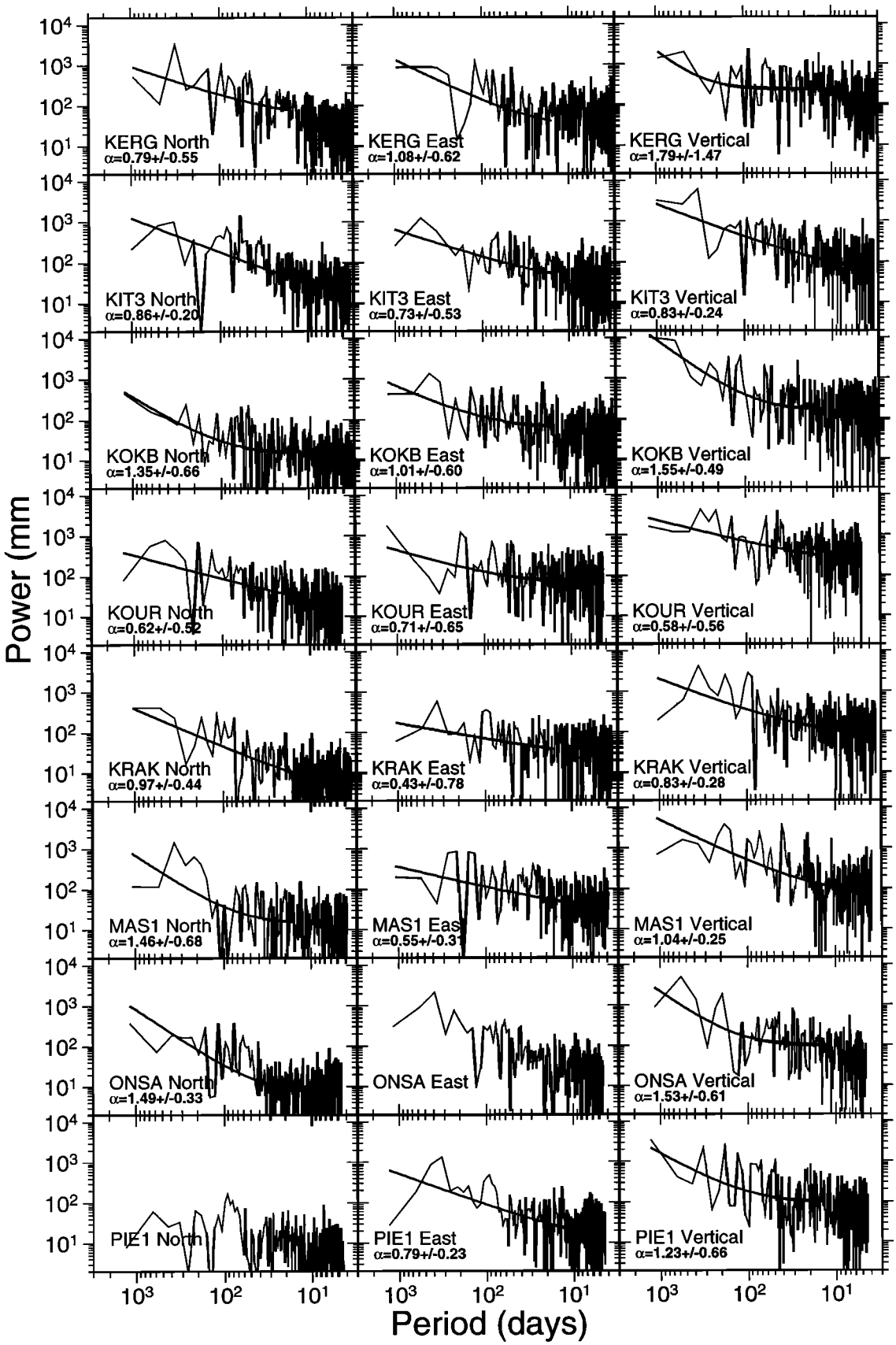

Figure 4. (continued)

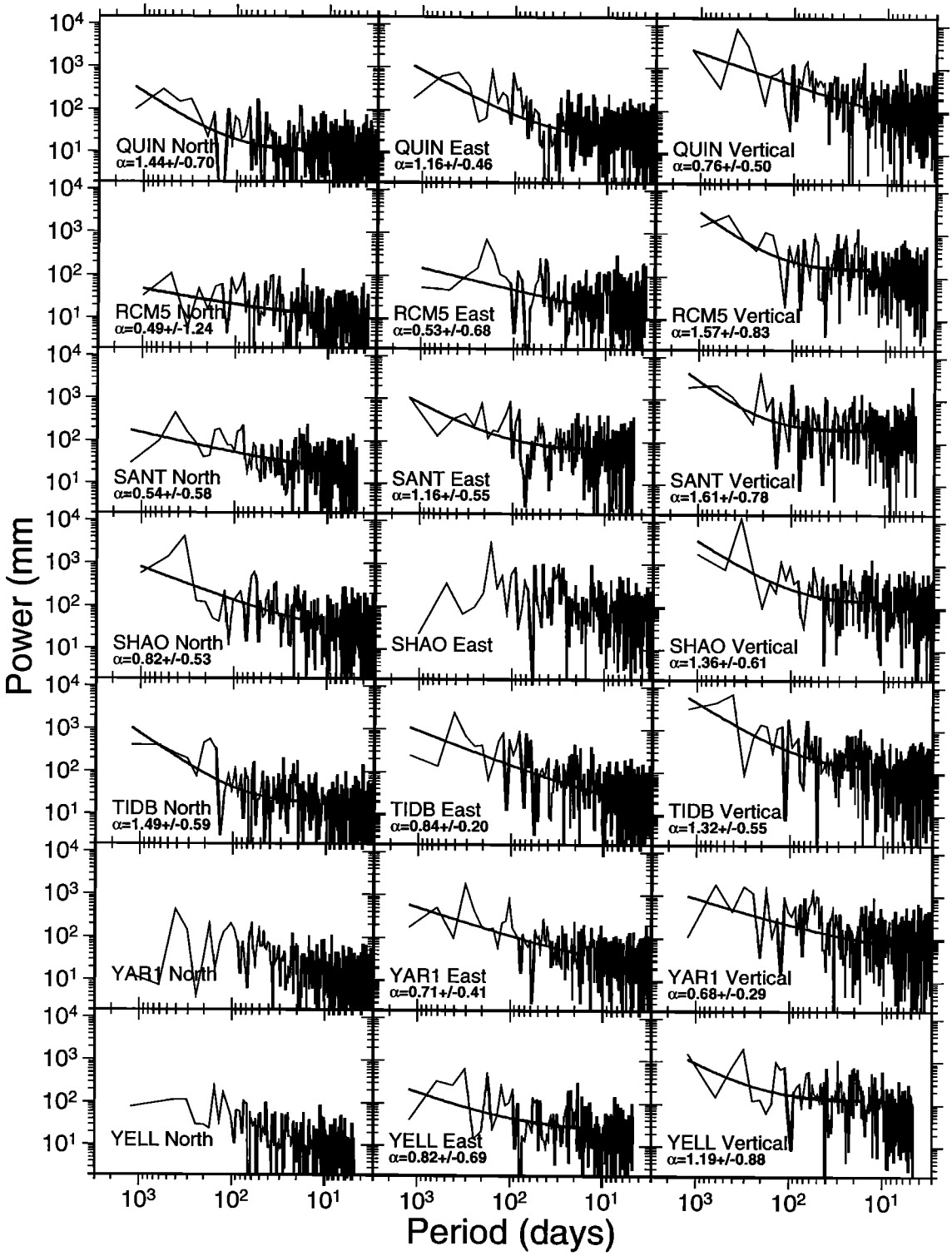

Figure 4. (continued)

here, we therefore retained the annual signature. However, for all other results (e.g., MLE) the annual term has been removed to avoid contaminating the low-frequency part of the power spectrum with a known signal, as the main focus of this study is to characterize random noise correlated over a long time span. Note that power at the annual period is clearly present in some of the spectra (e.g., vertical component of FORT and KRAK) but not in others (e.g., vertical component of BRMU, north component of ONSA). A few spectra (e.g., vertical component of MAS1) have peaks at the semiannual period.

Our mean spectral indices range from 0.74 to 1.02, depending on component, windowing technique, and whether the mean is weighted or unweighted. These values are bigger than the mean value 0.4±0.1 (one standard error) estimated by *Zhang et al.* [1997]. This difference may reflect one or more differences between the two analyses. First, Zhang et al. removed a common-

Table 5. Log Maximum Likelihood for Three Noise Models

	North		East		Vertical	
ID	W+F	W+RW	W+F	W+RW	W+F	W+RW
ALGO	121	92	45	32	73	48
BRMU	36	12	46	38	41	35
CASA	74	51	49	37	38	24
CMBB	56	47	27	16	78	58
FAIR	23	18	23	7	52	46
FORT	36	25	23	16	14	10
GOLD	13	3	34	27	73	65
GUAM	49	26	32	15	7	-1
KERG	100	83	22	18	27	12
KIT3	96	84	38	26	54	39
KOKB	59	39	37	21	97	89
KOUR	64	51	20	15	21	14
KRAK	79	70	15	7	21	12
MAS1	32	23	30	21	54	41
ONSA	76	74	59	47	67	54
PIE1	50	37	37	22	62	48
QUIN	53	38	51	42	63	45
RCM5	20	8	16	14	28	22
SANT	8	2	15	9	33	-12
SHAO	64	49	58	39	16	7
TIDB	113	97	88	67	125	107
YAR1	69	52	72	60	50	37
YELL	72	60	38	31	57	28

W+F, white noise plus flicker noise; W+RW, white noise plus random walk noise. Largest value gives preferred model. Values are normalized such that pure white noise model has likelihood=0.

mode error (due to orbits?) present in our data. Second, Zhang et al. were limited to 1.6 years of data; our longer time series may be more sensitive to long-term time-correlated noise. In the future, longer time series will undoubtedly enable more accurate estimates of time-correlated noise than those presented here. Third, Zhang et al. fit a straight line through the spectrum, while we fit a curve (equation (2)), allowing a better approximation to the low-frequency part of the noise spectrum. Zhang et al. also noted that a white plus flicker noise model fit their data.

Table 5 lists the difference of the log maximum likelihood among three models: white noise, white noise plus flicker noise, and white noise plus random walk noise. Larger values of the maximum likelihood indicate the preferred model [*Langbein and Johnson*, 1997; *Zhang et al.*, 1997], in this case, the white noise plus flicker noise model. We have not attempted to establish the statistical significance of a given numerical score returned by the MLE algorithm, as it requires a large number of computer-intensive simulations. Nevertheless, the fact that in every case tested (total 69) the white plus flicker noise model scored higher than the pure white noise or white plus random walk noise models argues strongly for the first model. Moreover, the same result is obtained from the spectral analysis. This is not to say random walk noise is not present in our time series. Rather, with the current data time span (3 years), current levels of white and flicker noise, and likely levels of random walk noise (1-3 mm/$\sqrt{\text{yr}}$ assuming monument noise of the type described by *Langbein and Johnson* [1997]), we are not able to detect it. Below, we discuss the time required to detect this level of random walk noise in time series of the quality currently available. In summary, both the spectral analysis and Maximum Likelihood Estimation are consistent with a white plus flicker noise model, and we adopt this noise model in the remaining discussion.

Table 6 lists the noise magnitude and standard deviation of white noise and flicker noise for the various time series. The annual signal is removed before estimating the noise components. Overall, noise in the east component is slightly higher than the north component, except ALGO and KIT3. The vertical component always has the largest white noise and flicker noise magnitude. The vertical component of CMBB has the largest flicker noise, which may be related to its older antenna and non-spherical radome (used at this site until August, 1997; Table 1) and/or possibly higher sensitivity to multipath due to antenna environment. Independent analyses have also indicated higher noise at this site [*Bar-Sever et al.*, 1998]. For individual components, there is no significant correlation between the magnitudes of white and flicker noise, but when all three components are plotted together, there is a good overall correlation (Figure 5). The mean white noise amplitudes are 3.3, 5.9, and 10.3 mm for the north, east, and vertical components. The corresponding flicker noise values are 5.7, 7.8, and 14.7 mm.

In order to test the possibility that our results are biased because our time series are too short, we applied our analysis to some GPS time series that are over 6.0 years in length analyzed in a similar way [M.Heflin, personal communication, 1997]. We found that the two results are very close for most of the sites (Figure 6), which suggests that our 3 year results adequately characterize the noise. However, higher (5-10%) amplitude flicker noise is observed in some of the longer (6.0 years) time series, perhaps indicating that longer time series are more sensitive to long period time-correlated errors. An alternate explanation is that the longer time series necessarily includes 1992 and 1993 data, which tend to be noisier than later data.

4.2. Regional Correlations

Figure 7 plots the white and flicker noise amplitudes as a function of station latitude. In general, latitudinal effects are small. While there is a slight tendency for southern hemisphere stations to have larger noise amplitudes, the difference is small and not statistically significant. On the other hand, tropical stations (between -23° and +23° latitude) clearly have higher levels of white noise in the vertical component compared to other stations (Figure 7). The difference is statistically significant at 95% confidence. Four stations (FORT, GUAM, KOUR, and KOKB) are in this latitude band. Two of these (FORT and GUAM) are equipped with newer Turbo Rogue receivers, one (KOUR) is equipped with the older Rogue receiver and one (KOKB) experienced a receiver upgrade (Rogue to Turbo Rogue) midway through the time series studied here with no obvious effects (Table 1, Figure 3). Thus the difference is unlikely to be due to hardware differences.

Inspection of time series from other stations in our database not analyzed for this report suggests the effect is real and not an artifact of small sample size. The weighted rms scatter (WRMS) in the vertical component is a reasonable proxy for white noise.

Table 6. Noise Amplitude

ID	North			East			Vertical		
	WRMS	σ_w	σ_f	WRMS	σ_w	σ_f	WRMS	σ_w	σ_f
ALGO	3.4	1.8±0.1	4.9±0.2	4.4	3.6±0.1	4.1±0.3	10.3	6.6±0.3	13.9±0.7
BRMU	3.6	2 6±0.1	4.2±0.3	6.6	5.1±0.2	5.6±0.5	12.5	10.0±0.3	10.8±1.1
CASA	4.2	2.5±0.1	5.3±0.3	6.9	5.1±0.2	6.8±0.5	12.5	9.4±0.3	12.4±0.9
CMBB	4.9	3.1±0.1	5.6±0.4	9.6	6.4±0.3	9.6±0.8	19.8	9.6±0.6	24.0±1.4
FAIR	4.0	3.0±0.1	3.9±0.4	5.3	3.5±0.2	5.8±0.5	13.7	8.2±0.5	15.2±1.3
FORT	5.9	4.2±0.2	5.9±0.5	9.2	7.5±0.3	7.3±0.8	19.0	15.7±0.5	12.3±1.8
GOLD	3.7	3.0±0.1	3.6±0.3	7.5	5.5±0.2	6.8±0.7	16.3	8.5±0.5	21.4±1.3
GUAM	7.0	4.4±0.2	9.2±0.6	12.3	8.9±0.3	14.7±1.1	19.0	16.7±0.5	14.5±2.1
KERG	8.3	4.8±0.2	10.4±0.6	10.0	8.5±0.3	7.7±0.8	15.2	12.0±0.4	15.9±1.4
KIT3	7.7	3.8±0.2	10.9±0.5	8.1	6.0±0.2	8.3±0.7	13.7	7.9±0.4	17.8±1.0
KOKB	4.5	3.2±0.1	5.4±0.3	8.7	6.5±0.2	8.8±0.7	17.2	12.1±0.4	17.5±1.3
KOUR	6.1	3.9±0.2	6.8±0.5	10.8	9.2±0.3	7.9±1.0	22.2	17.0±0.6	17.1±2.2
KRAK	4.3	2.9±0.1	4.7±0.3	6.9	5.6±0.2	6.2±0.7	14.2	11.3±0.4	12.5±1.3
MAS1	5.5	4.0±0.1	4.8±0.5	8.7	6.9±0.3	8.5±0.9	14.8	9.7±0.5	18.9±1.3
ONSA	4.3	2.7±0.1	4.7±0.3	6.7	3.9±0.2	8.0±0.5	10.2	6.4±0.3	12.1±0.9
PIE1	3.2	2.1±0.1	3.9±0.3	6.3	4.2±0.2	6.6±0.5	11.0	7.3±0.3	12.3±0.9
QUIN	4.1	2.9±0.1	4.8±0.3	7.1	5.4±0.2	6.5±0.5	13.9	9 9±0.3	13.4±1.0
RCM5	3.8	3.1±0.1	3.7±0.4	6.5	5.4±0.2	5.4±0.4	13.6	11.1±0.4	11.9±1.3
SANT	5.9	5.0±0.2	4.0±0.5	9.4	8.0±0.3	6.5±0.8	15.8	12.6±0.5	13.9±1.5
SHAO	7.8	5.1±0.2	8.4±0.6	10.7	7.2±0.3	14.0±0.8	14.2	11.3±0.3	10.3±1.3
TIDB	5.0	3.2±0.1	5.6±0.3	7.9	4.7±0.2	10.0±0.5	13.4	8.7±0.3	14.6±0.9
YAR1	4.5	3.0±0.1	5.8±0.3	7.2	5.0±0.2	8.1±0.4	12.1	9.0±0.3	13.3±1.0
YELL	3.6	2.0±0.1	4.5±0.2	5.3	3.8±0.2	5.2±0.5	10.1	6.2±0.3	12.4±0.8
Mean	5.0	3.3±0.9	5.7±2.1	7.9	5.9±1.7	7.8±2.5	14.6	10.3±3.0	14.7±3.4

Noise amplitude is in mm. WRMS, Weighted rsms.

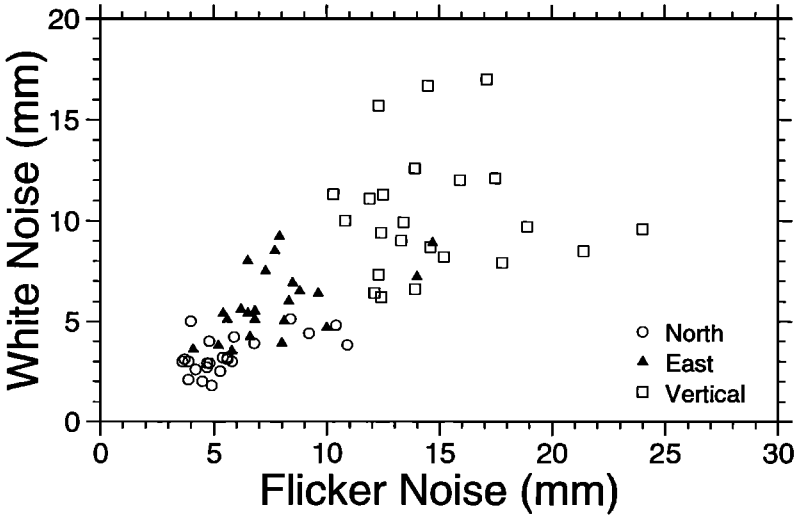

Figure 5. White noise versus flicker noise amplitude for the 23 GPS time series.

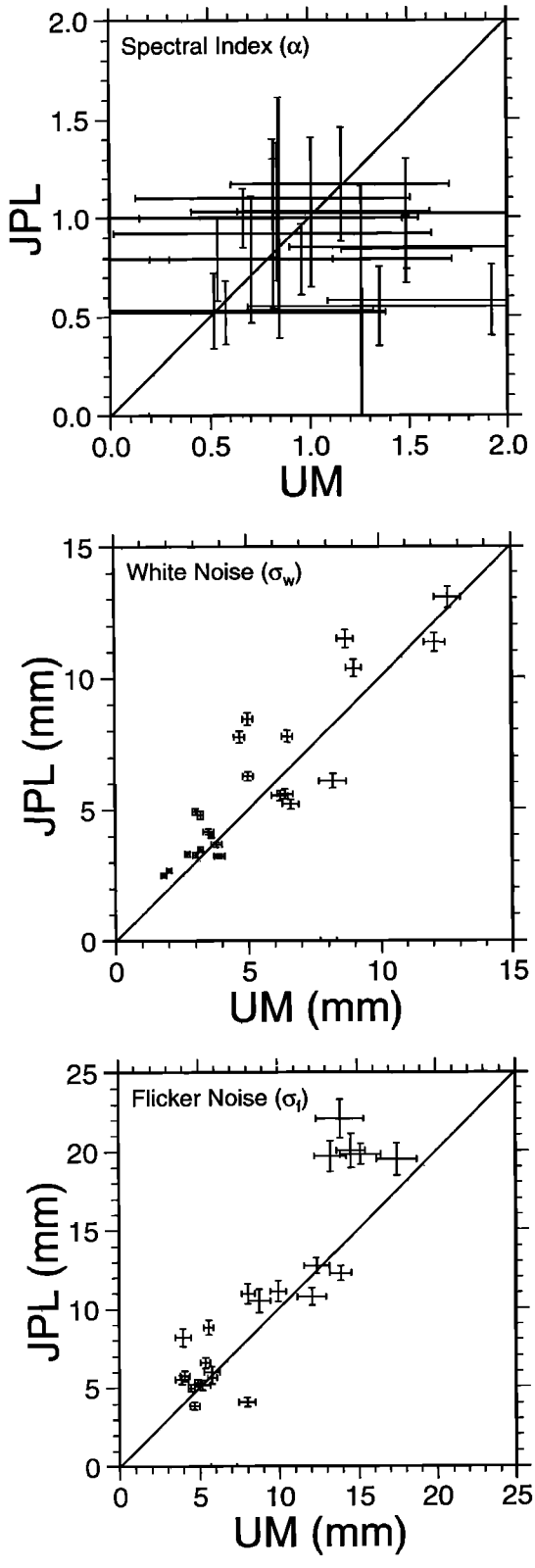

Figure 6. Comparison of spectral index (α) and amplitude of white and flicker noise computed for 3 year time series (this study) and 6 year time series (M.*Heflin*, personal communication, 1997) for sites where both are available. The solid line has a slope of 1.00. One standard error bars are also shown.

The four tropical stations in Table 6 have WRMS values in the vertical component of 19.4 mm, while the 18 nontropical stations (excluding CMBB) have mean vertical WRMS ranging from 10 to 16 mm (mean = 13.2 mm). Eight other tropical stations in our database not used in this analysis and not affected by antenna changes have WRMS values ranging from 15 to 29 mm (mean = 18.2 mm).

Several explanations seem plausible. Perhaps the additional noise is related to tropospheric water vapor, which exhibits higher levels and higher variability in tropical regions [e.g., *Dixon and Kornreich Wolf*, 1990] and thus is more sensitive to mismodeling. Note that any atmospheric effects in our time series are residual, representing the effects of atmospheric delay unmodeled in the estimation process. Another possibility is that the additional white noise in the vertical component is related to environmental effects near the antenna that are more common in the humid tropics. High moisture on the antenna housing or antenna element might promote elevation angle-dependent phase errors. Elevation angle-dependent errors tend to affect the vertical component more than the horizontal components. For example, we have observed mold growing on one side of a plastic antenna cover in one tropical station within one year of installation.

Table 7. Velocity Error Estimates for White and White Plus Flicker Noise Models

ID	North		East		Vertical	
	W	W+F	W	W+F	W	W+F
ALGO	0.1	1 1	0 2	0 9	0 4	3.1
BRMU	0.1	0.9	0.3	1.2	0.5	2.4
CASA	0.2	1.2	0.3	1.5	0.5	2 8
CMBB	0.3	1 4	0.5	2.4	1 1	5.7
FAIR	0.2	0.9	0.3	1 3	0 8	3.5
FORT	0.2	1.2	0.4	1.5	0.8	2 6
GOLD	0 2	0.8	0.3	1.5	0.7	4.6
GUAM	0 4	2.5	0.6	4.1	1.0	4.1
KERG	0 4	3.0	0.5	2.3	0.8	4.6
KIT3	0.4	3.0	0.5	2.4	0.8	5.0
KOKB	0.2	1.2	0.3	2.0	0.7	3.9
KOUR	0 3	1.5	0.5	1.8	1.0	3.8
KRAK	0.2	1.2	0.4	1.7	0.7	3.4
MAS1	0.4	1.4	0.6	2.4	1.0	5.2
ONSA	0.3	1.2	0.4	2.0	0 6	3 0
PIE1	0.1	0 8	0.3	1 4	0 5	2.7
QUIN	0.2	1.1	0.3	1.5	0 5	3.0
RCM5	0.2	1.1	0.4	1.6	0.8	3.5
SANT	0.3	0 9	0.4	1.5	0.7	3 1
SHAO	0.4	2.3	0.5	3 8	0.7	2.9
TIDB	0.2	1.3	0.3	2 2	0 5	3.3
YAR1	0.2	1.3	0.3	1.8	0.5	3.0
YELL	0.2	1.0	0.3	1.2	0 5	2.8

Velocity error estimates are in mm/yr.

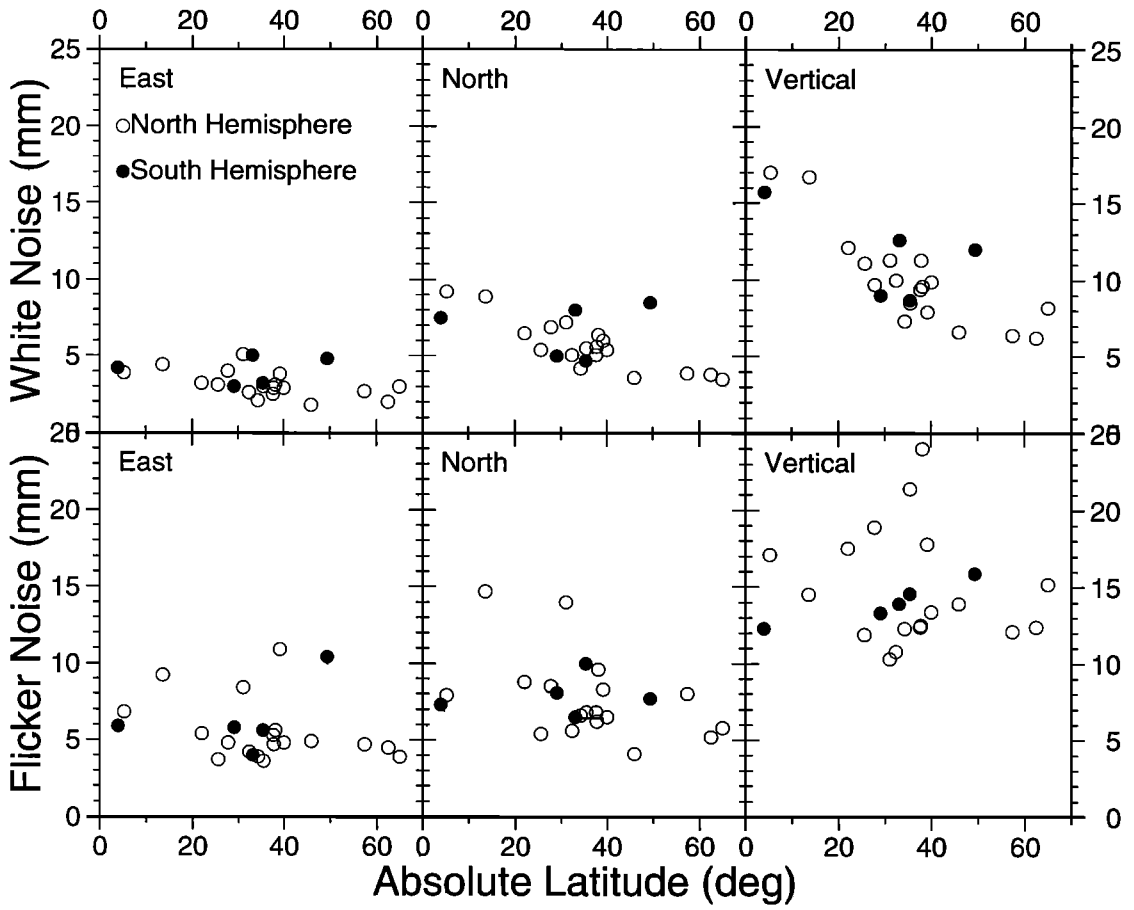

Figure 7. White and flicker noise (Table 6) as a function of absolute latitude. Error bars for these data are of the order of the symbol size and are omitted for clarity.

Inspection of Table 6 suggests another possible regional variation in noise. Stations in North America and western Europe tend to be less noisy than stations in other areas. While this might reflect tracking station density (influencing the quality of satellite ephemerides?), it could be an artifact of our small sample size or may simply reflect greater resources available to maintain and replace older equipment.

4.3. Effect of Time Correlated Noise on Velocity Error Estimates

The standard error of a rate (σ_r) estimated in a linear regression of evenly spaced measurements can be expressed for pure white noise as [*Zhang et al.*, 1997]

$$\left(\sigma_r\right)_w \cong \frac{2\sqrt{3}\sigma_w}{N^{1/2}T} = \frac{2\sqrt{3}\sigma_w}{f_s^{1/2}T^{3/2}} \qquad N >> 1 \qquad (18)$$

and for random walk noise as

$$\left(\sigma_r\right)_{rw} \cong \frac{\sigma_{rw}}{T^{1/2}} \qquad N >> 1 \qquad (19)$$

where T is the time span, f_s is the sampling frequency, and σ_w and σ_{rw} are the standard deviations of white and random walk noise. There is no exact analytical expression for flicker noise; its effect on rate uncertainty has been calculated numerically. For pure white noise the rate error depends on time span as $1/T^{3/2}$, while for random walk noise the rate error goes as $1/T^{1/2}$ and is not dependent on sampling frequency at all. For flicker noise the rate error depends on these parameters in an intermediate way. For example, the time span dependence is $\sigma_r \approx \sigma_f/T$. Figure 8a shows the effects of various combinations of white, flicker, and random walk noise on rate estimates based on linear regression for time series of different lengths using typical white and flicker noise values derived from this study. The rate uncertainties decrease more slowly for time series containing significant time-correlated noise, especially for time series that are long compared to the crossover period (the point where the contributions of white noise and time-correlated noise are equal). The velocity errors of GPS sites based on the model of white noise plus flicker noise are listed in Table 7. If only white noise is assumed, velocity errors are underestimated by factors of 5-11.

An approximate expression for total rate error, valid for evenly spaced measurements, can be obtained by summing the variances (σ^2) from (18) and (19) and adding an expression for the variance contribution from flicker noise:

$$\sigma_r \cong \left(\frac{12\sigma_w^2}{gT^3} + \frac{a\sigma_f^2}{g^bT^2} + \frac{\sigma_{rw}^2}{T}\right)^{1/2} \qquad (20)$$

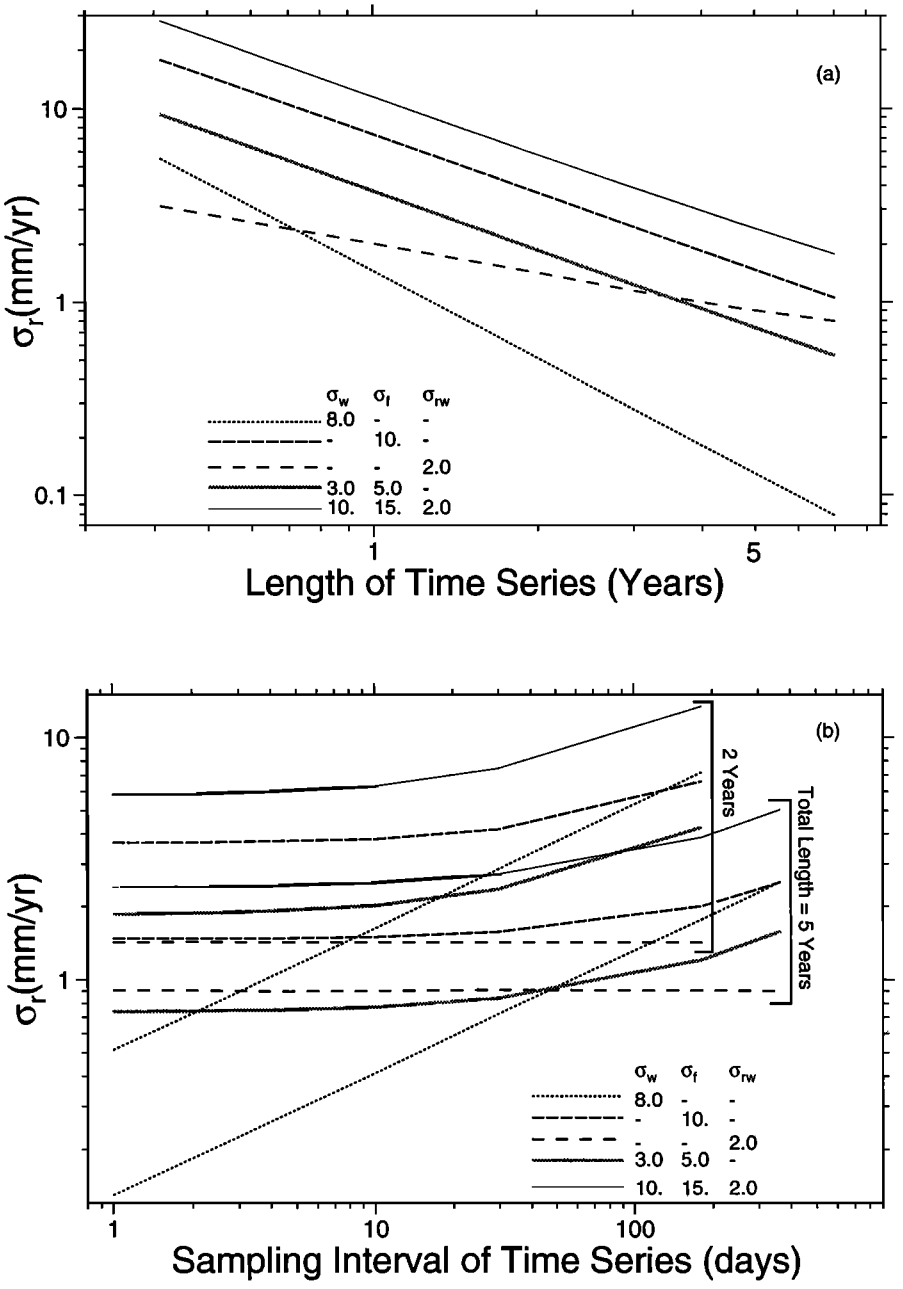

Figure 8. Velocity errors for time series with different lengths (Figure 8a; daily sampling) or sampling intervals (Figure 8b). In addition to time series of pure white noise, flicker noise, and random walk noise, the table also shows the "average best case" ($\sigma_w = \pm 3$ mm, $\sigma_f = \pm 5$ mm) and "average worst case" ($\sigma_w = \pm 10$ mm, $\sigma_f = \pm 15$ mm, $\sigma_{rw} = \pm 2$ mm/$\sqrt{\text{yr}}$) on the basis of Table 6 and *Langbein and Johnson* [1997].

where g is the number of measurements per year, T is the total time span in years, σ_w and σ_f are the magnitudes of white and flicker noise in mm, σ_{rw} is the random walk noise in mm/$\sqrt{\text{yr}}$, and a and b are empirical constants. By comparison with the numerical results shown in Figure 8, we obtain $a \approx 1.78$ and $b \approx 0.22$. For stations not analyzed in this report, an estimate of the total rate error can be made using (20), the regional average noise values compiled in Table 8, and values for random walk noise in the range 1-4 mm/$\sqrt{\text{yr}}$ [*Langbein and Johnson*, 1997].

Assuming that monument noise can be characterized as a random walk, and assuming that a typical magnitude for this process is 2.0 mm/$\sqrt{\text{yr}}$ [*Langbein and Johnson*, 1997], we can estimate the time required before the velocity estimates become sensitive to this source noise, i.e., the crossover period. For time series with relatively high levels of white and flicker noise (e.g., 10 and 15 mm, respectively, in Figure 8a), more than 15 years is required. For lower levels of white and flicker noise (e.g., 3 and 5 mm, respectively, in Figure 8a) the velocity estimates are sensitive to random walk monument noise within about 4 years. For short baselines [e.g., *Dixon et al.*, 1997] or dense networks where common-mode error reduction can be exploited [*Wdowinski et al*, 1997] the effects of monument noise may be manifested sooner than 4 years.

An informal test of the noise model can be performed by fit-

Table 8. Mean and Standard Deviation for White and Flicker Noise by Region

	White, mm			Flicker, mm		
	North	East	Vertical	North	East	Vertical
Tropical	3.9±0.5	8.0±1 3	15.4±2.3	6.8±1.7	9.7±3.4	15.4±2.4
North America, Western Europe[a]	2.6±0.4	4.6±0.8	8 6±1.9	4.4±0.6	6 3±1.1	13.5±2.9
Other	4.1±0.9	6.6±1.4	10.2±1.8	7.1±2.8	9.0±2.4	15.1±2 6

N, north; E, east; V, vertical
[a]Omits CMBB.

ting the velocity data and modeled errors for sites on the stable interior of a plate to a rigid plate model. Assuming that the plate is perfectly rigid, the average velocity residual (observed velocity minus the velocity predicted by the best fit Euler vector) should approximately reflect the modeled noise, and the reduced chi-square statistic (chi-square per degree of freedom, a measure of goodness of fit) should be of order unity. *Mao* [1998] fit the velocity of 19 sites located on stable North America with at least 1.6 years of data to a rigid plate model, obtaining a reduced chi-square of 28.9 (white noise model) and 1.28 (white plus flicker noise model). With a slightly different subset of data (16 sites on the stable plate interior, all with time series 2.0 years or longer) we obtain a reduced chi-square of 0.80 with the white plus flicker noise model. These tests confirm our expectation that a pure white noise model underestimates total velocity error, and suggests that our new noise model, accounting for time correlated noise, accurately estimates total velocity error for the current coordinate velocity data set.

The effect of sampling interval is clear from Figure 8b and the form of (20). A high sampling rate reduces white noise and flicker noise, although it is less efficient for the latter, but has no effect in the case of random walk noise. Continuous measurements are nevertheless important, as they are the best way to measure, understand, and hopefully reduce time-correlated noise.

5. Conclusions

1. Spectral analysis of coordinate time series spanning 3 years from globally distributed GPS sites suggests that the noise characteristics of all three components can be modeled by a combination of white plus flicker noise.

2. Both white and flicker noise amplitudes increase in the order north, east, and vertical.

3. The white noise part of the vertical component is higher for tropical (±23° latitude) stations than mid-latitude and high-latitude stations.

4. Southern Hemisphere stations are not significantly noisier than Northern Hemisphere stations.

5. The velocity error in coordinate time series may be underestimated by factors of 5-11 if a pure white noise model is assumed.

6. Longer time series than those presented here will be required to accurately assess random walk noise in GPS coordinate time series.

Acknowledgments. We thank John Langbein, Jorge Willemsen, Hadley Johnson, Tom Herring, and Jie Zhang for generously sharing their knowledge of time-correlated noise, John Langbein for providing his MLE software, and Yehuda Bock for sharing preprints of his papers before publication. Langbein, Johnson, and Bock also provided thorough reviews which greatly improved the paper. We also thank the IGS for making data from a large number of stations publicly available. Most figures for this paper were generated by GMT [*Wessel and Smith*, 1995]. This work was supported by NASA's Earth System Science Fellowship to Mao and several NASA grants to Harrison and Dixon.

References

Agnew, D.C., The time-domain behavior of power-law noises, *Geophys. Res. Lett.*, *19*, 333-336, 1992.

Bar-Sever, Y.E., P.M. Kroger, and J.A. Borjesson, Estimating horizontal gradients of tropospheric path delay with a single GPS receiver, *J. Geophys. Res.*, *103*, 5019-5035, 1998.

Brockwell, P J , and R. A Davis, Introduction to Time Series and Forecasting, 420pp., Springer-Verlag, New York, 1996.

Boucher, C., Z. Altamimi, M. Feissel, and P. Sillard, Results and analysis of the ITRF94, 191 pp., *Tech. Note 20, Int. Earth Rotation Serv*, 1996.

Dixon, T.H., A. Mao, M. Bursik, M. Heflin, J. Langbein, R Stein, and F. Webb, Continuous monitoring of surface deformation at Long Valley Caldera, California, with GPS, *J. Geophys. Res.*, *102*, 12,017-12,034, 1997.

Johnson, H.O., and D.C. Agnew, Monument motion and measurements of crustal velocities, *Geophys Res. Lett.*, *22*, 2905-2908, 1995.

Johnson, H. O., and F. K. Wyatt, Geodetic network design for fault mechanics studies, *Manuscr. Geod*, *19*, 309-323, 1994.

Koch, K.R., Maximum likelihood estimate of variance components, *Bull Geod.*, *60*, 329-338, 1986.

Langbein, J., and H. Johnson, Correlated errors in geodetic time series: Implications for time-dependent deformation, *J. Geophys. Res*, *102*, 591-604, 1997.

Langbein, J , F. Wyatt, H. Johnson, D. Hamann, and P Zimmer, Improved stability of a deeply anchored geodetic monument for deformation monitoring, *Geophys. Res. Lett*, *22*, 3533-3536, 1995.

Lomb, N.R., Least squares frequency analysis of unequally spaced data, *Astrophys. Space Sci.*, *39*, 447-462, 1976.

Mao, A., Geophysical applications of the Global Positioning System. Ph. D. dissertation, University of Miami, 149 pp., 1998.

Press, W.H., B.P. Flannery, S.A. Teukolsky, and W.T. Vetterling, *Numerical Recipes*, 818 pp., Cambridge Univ Press, New York, 1992.

Scargle, J.D., Studies in astronomical time series analysis, II, Statistical aspects of spectral analysis of unevenly spaced points, *Astrophys. J.*, *263*, 835-853, 1982.

Wdowinski, S., Y. Bock, J. Zhang, P. Fang, and J. Genrich, Southern California Permanent GPS Geodetic Array· Spatial filtering of daily positions for estimating coseismic and postseismic displacements induced by the 1992 Landers earthquake, *J. Geophys Res.*, *102*, 18,057-18,070, 1997.

Wessel, P , and W. H F. Smith, New version of the Generic Mapping Tools released, *Eos Trans. AGU, 76 (33)*, 329-330, 1995.

Zhang, J., Y. Bock, H Johnson, P. Fang, S. Williams, J. Genrich, S.

Wdowinski, and J Behr, Southern California Permanent GPS Geodetic Array: Error analysis of daily position estimates and site velocities, *J. Geophys. Res.*, *102*, 18,035-18,055, 1997.

Zumberge, J. F , M. B. Heflin, D. C. Jefferson, M. M. Watkins, and F. H. Webb, Precise point positioning for the efficient and robust analysis of GPS data from large networks, *J. Geophys. Res.*, *102*, 5005-5017, 1997.

T. H. Dixon and C. G. A. Harrison, Marine Geology and Geophysics Division, Rosenstiel School of Marine and Atmospheric Science, University of Miami, 4600 Rickenbacker Causeway, Miami, FL 33149-1098 (tim@corsica.rsmas.miami.edu; charrison@rsmas.miami.edu)

A. Mao, Magellan Systems Corporation, 960 Overland Court, San Dimas, CA 91773.

(Received February 11, 1998; revised September 16, 1998; accepted September 28, 1998)